









# Predicting Delamination in Concrete Bridge Decks from Ground Penetrating Radar Signals using Machine Learning

## Authors

---

- **Ishfaq Aziz**  
 [0000-0001-5723-0331](#) ·  [ishfaq2](#)
- **Jesus Castro**  
 [0000-0002-7684-7422](#) ·  [jcastr54](#)
- **Chirayu Kothari**  
 [0000-0003-4468-1138](#) ·  [ck0103](#)
- **Omar Abdelrahman**  
 [0000-0003-0618-8481](#) ·  [oaa4](#)

# Introduction

---

The data set represents raw signals of Non-Destructive Evaluation (NDE) tests conducted by Ground Penetrating Radar (GPR) which were collected from in-service reinforced concrete bridge decks. The dataset was annotated using three classes in accordance with bridge deck repair: Class 1-No Delamination; Class 2-Delamination (delamination above top bar mat), and Class 3-Delamination (delamination below top bar mat).

The data will be obtained from <https://commons.und.edu/data/19/> [1] which contains annotated dataset for the structural defects. Data is present in the .xlsx format. Each column in the dataset has an approximate length of 512 where the first column represents the time (ns), and the rest of the columns are all amplitudes of GPR signals. Hence, each raw signal (columns) is directly annotated to one of the three possible classes. In addition, some other information like the scan length and the coordinates of each signal scan is also provided.

Ground Penetrating Radar (GPR) is an imaging technique that uses wide-band sinusoidal electromagnetic waves, with frequencies ranging from 0.5 to 2 GHz, to produce high-resolution images of the subsurface materials. GPR is an effective tool for subsurface inspection and quality control on engineering construction projects. The survey method is rapid, nondestructive, and noninvasive. Interpretation of GPR data commonly helps to evaluate and measure different properties of a concrete structure.

The data collected from the GPR are usually presented in two different formats, A-scan and B-scan. Most modern devices have the capability to present the two formats simultaneously. The A-scan is the raw signal of energy received by the antenna shown as a function of time and signal strength (amplitude). The received signal in Figure 1a is an example of an A-scan. The B-scan, also known as radargram, is constructed from the sequence of multiple A-scans related to the position of the antenna, as shown in Figure 1b, where the depth is represented on the y-axis and the survey distance is shown on the x-axis orthogonal to the y-axis. The amplitude of the received signal is often shown as a color-coded intensity plot, often in grey, as shown in Figure 1c. B-scans are usually visually inspected to identify and locate any delamination within the concrete or to locate the reinforcement rebars.

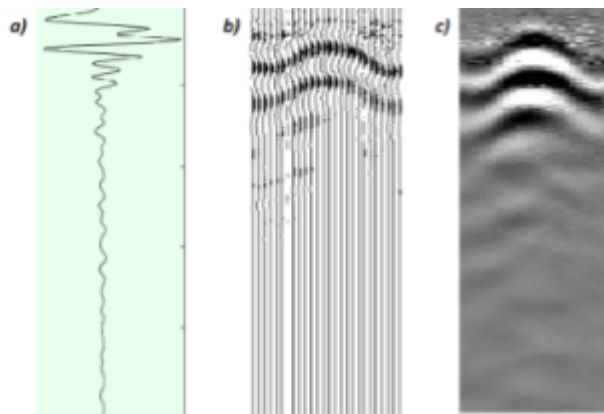


**Figure 1: a) Single wave signal (A-scan). b) Collection of signals across a distance along the surface. c) Color intensity plot of (b) (B-scan).**

## Plan

---

The A-scan data is categorized into three classes based on the delamination conditions. Fast Fourier transform of the A-scans will be performed to obtain the peak frequency and peak width. These values will act as independent variables in the machine learning model to predict the delamination condition. The bridge health at each location where an A-scan is collected is categorized into three classes: Class 1 No delamination, Class 2 Delamination (above the top bar mat), and Class 3 Delamination (below the top bar mat). Around 10,000 labeled A-scans will be used to train the model

and 3000 labeled A-scans will be utilized for validation. Later, the trained model will be tested on 3000 A-scans to predict the delamination condition. Finally, B-scans will be generated and deck conditions at different locations of the bridge will be predicted.

# Exploratory Data Analysis

## Preliminary Analysis

The dataset consists of 16,384 GPR scans that were taken at different locations along the bridge. Each scan has a total of 512 points representing a scan time of 12 ns. The scans are categorized into three main classes: Class 1 – no delamination, class 2 – delamination above the top rebar, and class 3 – delamination below the top rebar, representing 8427, 6812, and 1144 scans, respectively, as shown in Table 1. Other properties of the GPR scans are summarized in Table 2.

Table 1. Summary of classes/labels of the dataset

| Classes                       | Class 1        | Class 2                                    | Class 3                                    |
|-------------------------------|----------------|--|--|
| No of scans                   | 8427           | 6812                                       | 1144                                       |
| Meaning of each class         | Sound Concrete | Concrete with delamination above top rebar | Concrete with delamination below top rebar |
| Peak amplitude of mean signal | 10121          | 9813                                       | 9649                                       |

Table 2. Properties of the GPR scans

| Parameter                         | Value           |
|-----------------------------------|-----------------|
| Total number of scans             | 16,383          |
| Total Length of scan              | 363.3 ft.       |
| Interval between subsequent scans | 0.0222 ft.      |
| Time duration of each scan        | 12 nano seconds |
| Data points per scan              | 512             |
| Sample rate (calculated)          | 42.67 GHz       |

The amplitudes of the signals in the dataset were found to have high numerical values. The average amplitude of the whole dataset is around 33,000. So, in order to make the data more symmetric around the x-axis, the average of the first few nanoseconds of readings was subtracted from the whole dataset, resulting in scans that start with amplitudes close to zero. Figure 2 shows one randomly selected scan from each of the three classes.



Figure 2: Randomly selected signals from each of the three classes

Based on the reference paper that was used to obtain the data [1] the B-scan, which is a visual representation of a combination of individual scans stitched together, showed that the bottom rebar reflection was detected at around 7 ns. Thus, it was decided that the readings after around 8 ns would not be useful for the purpose of our model and the remaining 4 ns were removed. Also, it was observed that the initial reflection from the top surface of the concrete is detected around 2 ns, so the first 2 ns were also removed from our data. Sample scans from the resulting signal are shown in Figure 3.



**Figure 3: Randomly selected signals from each class, showing only the data points between 2 and 8 ns.**

## Mean Plots

To visually distinguish between the three different classes of data, the mean all scans from each class are plotted in Figure 4. The figure shows that the three means look almost identical to each other, so there is no distinctive feature in the time domain signal that can help assign new signals to any of the three classes. Thus, deeper levels of data analysis are required to identify any distinctive features that can help classify new data.



**Figure 4: The mean of all signals for each class.**

## Fast Fourier Transform (FFT)

Another approach to visualizing sinusoidal time-series datasets is by identifying dominant cyclic patterns. This can be conducted with the Fast-Fourier Transform, a computationally efficient way to calculate the discrete Fourier Transform from a dataset. This algorithm transforms information on the time domain into the frequency domain.

The time-series datasets from the three classes (no delamination, delamination above rebar, and delamination below rebar) were all transformed into the frequency domain to identify patterns that could easily differentiate one class from another. As observed in Figure 5, most of the signal amplitude peaks are observed at a frequency of approximately 0.8 GHz, which is in the standard operating frequency range of GPR antennas for concrete testing.



**Figure 5: Amplitude vs Frequency Class 1 with no delamination**

In Figure 6 it is observed that in the sections where delamination was identified above the top rebar layer, the amplitude peaks were higher in magnitude than the observed peaks in the sections with non-delaminated sections at similar frequencies. On the other hand, the plot corresponding to the amplitudes of sections identified with delamination below the top rebar later (Figure 7.) displays amplitude peaks with magnitudes lower than in Figure 5 and Figure 6.



**Figure 6: Amplitude vs Frequency Class 2 with delamination above the rebar**

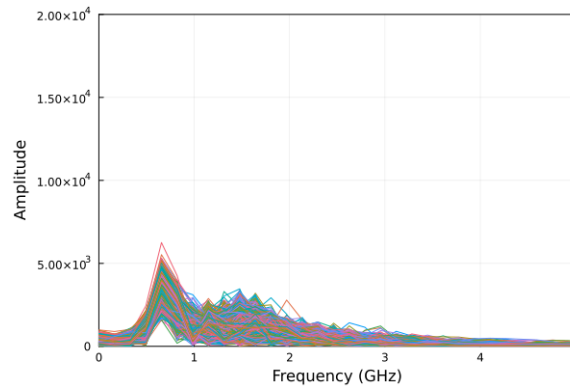


**Figure 7: Amplitude vs Frequency Class 3 with delamination below the top rebar**

From this data processing approach (FFT), a sound differentiation from the three classes (beyond the observed magnitudes in amplitude at approximately 0.8 GHz) cannot be concluded. Furthermore, the maximum amplitude of the FFT data and the frequency corresponding to the maximum amplitude was plotted (Figure 8). It was observed that the maximum amplitude of most of Class 1 and Class 2 was similar. However, some of the FFT spectra in Class 2 had higher amplitude than that of Class 1. Also, some of the FFT spectra in Class 2 had amplitude close to the mean of Class 3. It can potentially be attributed to the labeling of data.



**Figure 8: Violin plots representing the variation in maximum FFT amplitude of the three classes.**

Similarly, the frequency at maximum amplitude was observed for the FFT spectra in the three classes (Figure 9). The mean frequency at maximum amplitude for class 3 was lower than that of class 2 and class 1. The Violin plot for class 1 and class 2 look similar. However, some of the FFT spectra in class 2 have a frequency at a maximum amplitude lower than that of class 1's data.

**Violin plot representing the variation in frequency at maximum FFT amplitude of the three classes.** ](<https://user-images.githubusercontent.com/112973477/198889398-21f6da40-2975-4964-b01e-6223ac78a1ce.png> "Tall image")  
{#fig:tall-image height=2in}

It can be easier to separate out Class3 from Class 1 and Class 2 based on the FFT analysis.

## Principal Component Analysis

Principal component analysis (PCA) was performed on the dataset to change the basis of the data and improve its interpretability. The number of modes was selected to be 2. The results of the first and second modes of the PCA data of the whole dataset are plotted in Figure 10. Since the number of data points for each class is different, normalizing the number of points might provide a better visual representation of the scatter of data of different classes. So, 1000 random points were selected from each class and then PCA was performed on this sub-dataset. The results of the two modes of this PCA are shown in Figure 11.

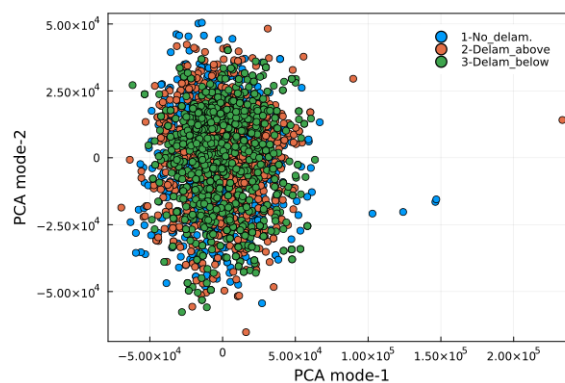


**Figure 9: The PCA data for all the datasets.**

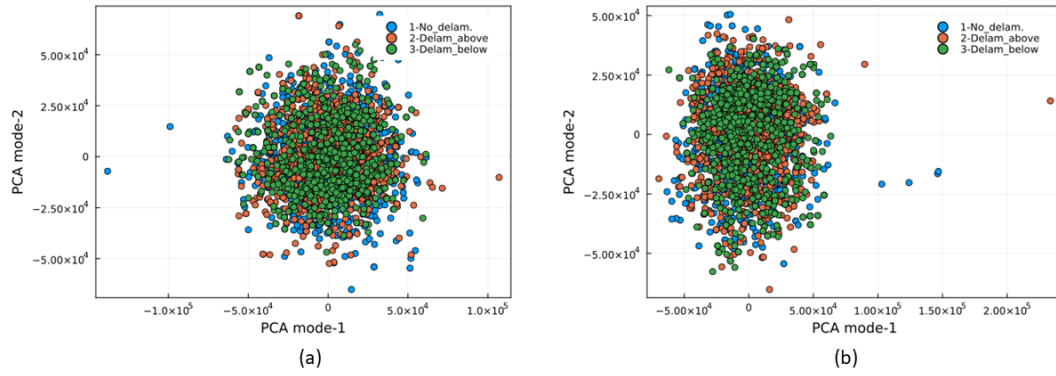


**Figure 10: PCA data of two different 1000 randomly selected points from each class.**

## Predictive Modeling

Based on the exploratory data analysis it can be concluded that the differentiation of the classes is challenging. The analytical approach to determining key features for distinguishing different classes is not conclusive and overall, the data delineation is not observed. Hence, Convolutional Neural Network (CNN) will be used to classify the delamination into three categories. The dataset will be divided into two parts with 60-70 % of the data used for training and the rest 30-40% dataset for validation. The raw A-scans will be given as input to the CNN network and will be trained for the expected outcomes in terms of different delamination classes.

Furthermore, the input parameters from our exploratory data analysis (maximum amplitude in time and frequency domain, PCA modes, etc.) will be used to create a machine-learning model for the prediction of the delamination category of the A-scan taken by GPR. Both models will be compared with each other in terms of accuracy and precision.

## References

[1] Ichi, E., & Dorafshan, S. (2021). SDNET2021: Annotated NDE Dataset for Structural Defects, 10.31356/data019

[2] Scheers, B., 2001. Chapter 2. Ground penetrating radar. In: Ultra-Wideband Ground Penetrating Radar, with Application to the Detection of Anti-Personnel Landmines. Brussels: s.n., pp. 2-1 -2-43.